

Feasibility study on nearly-fuel-free planetary exploration with low-ballistic-coefficient aerocapture of sail-type vehicle

Kojiro Suzuki¹ and Kumiko Nakamura²

¹Professor, Department of Advanced Energy, Graduate School of Frontier Sciences, The University of Tokyo, 5-1-5 Kashiwanoha, Kashiwa, Chiba 277-8561, Japan, kjsuzuki@k.u-tokyo.ac.jp

²Graduate Student, Department of Aeronautics and Astronautics, Graduate School of Engineering, The University of Tokyo

Abstract

A novel concept of the nearly-fuel-free planetary exploration by the sail aerocapture vehicle, which uses the sail not only for the solar sailing but also for an aerodynamic decelerator at the orbit insertion, and its design methodology are presented. Considering a mission to Saturn, the trajectory analysis shows that the corridor of the entry path angle for successful aerocapture is significantly widened and that the aerodynamic heating is much reduced, thanks to the ultra-low ballistic coefficient of the sail-type vehicle. The coupled analyses of the rarefied flow field and the deformation of the sail demonstrate that the solar sail vehicle can survive under the condition of the aerodynamic heating and the stress due to the aerodynamic force. To sustain the disk-like shape of the sail during the atmospheric flight, an inflatable torus attached as a hoop support is recommended as well as a spin motion producing the centrifugal force.

1. INTRODUCTION

Planetary exploration has been attracting our scientific interest for a long time. For better understanding about a planet, observation from its orbit is preferable in comparison with fly-by missions. In general, however, such orbiter missions require high cost, because the rocket fuel for the orbit insertion must be additionally brought to the planet and, as a result, both a spacecraft and its launch vehicle become so heavy. For a planet with an atmosphere, the aerocapture [1], in which the spacecraft directly enters the planetary atmosphere from the interplanetary trajectory and uses the aerodynamic drag to obtain deceleration necessary for the orbit insertion by a single atmospheric pass, is known to be a promising technique to save the spacecraft fuel significantly. The payload capability will be augmented in comparison with the conventional vehicle using the propulsive orbit insertion. However, both very tight constraints on the atmospheric entry path angle for successful aerocapture under large uncertainty in the properties of the planetary atmosphere and the severe aerodynamic heating, which requires a heavy thermal protection system (TPS), prevent us from realizing it. For the aerocapture technique to be feasible, some breakthrough both in the vehicle design and in the trajectory design is necessary.

In the analysis of the atmospheric entry trajectory, the ballistic coefficient defined as:

$$C_B = \frac{m}{C_D S} \quad (1)$$

where m , S , C_D are the vehicle mass, area and the drag coefficient, respectively, is the most dominant parameter. One promising method to solve to the above problems is to use a low-ballistic-coefficient vehicle, which will be decelerated at higher altitudes than a conventional atmospheric entry vehicle. The flight at higher altitudes results in lower aerodynamic heating on the body, because the atmospheric density is lower there. To realize a low ballistic-coefficient, a vehicle must have a large area with a small mass. For this purpose, the membrane structure with some supporting device seems promising. For the earth's reentry, a vehicle with a large and lightweight deployable aeroshell made from high-temperature membrane materials has been considered by the authors' research group to reduce both the

aerodynamic heating and the mass for the thermal protection system [2]. For a Jovian entry probe, a balloon-type vehicle with the ballistic coefficient 1 kg/m^2 or lower is proposed [3]. Such advantages of a low-ballistic-coefficient vehicle are also attractive in the case of the aerocapture.

On the other hand, the solar sail [4] is attracting our attention as a “realistic” space propulsion system because of the recent rapid advancement in the membrane material technology. For example, the solar sail is considered for exploration of the inner solar system [5] and the rim of the solar system [6]. The solar sail vehicle generates the propulsive force by the reflection of the sunlight at the sail surface. Hence, it does not require any fuel for propulsion. To obtain the acceleration necessary for the interplanetary travel by the solar sail, both significantly large area and significantly small mass are essential, because the solar radiation pressure is quite small (only 4.6 N/km^2 on the earth’s orbit [7]). To receive the high solar radiation pressure, the sail must be made from a heat-resisting material, like Kapton® by DuPont™, and fly close to the sun. Such huge, lightweight and highly heat-resisting solar sail seems suitable also for a decelerator of a low-ballistic-coefficient atmospheric flight of the aerocapture. The solar sailing technique is well known as the fuel-free propulsion in the interplanetary space. On the other hand, the aerocapture is an orbital insertion technique without using a fuel. Consequently, a nearly-fuel-free orbiter mission for planetary exploration is expected to become possible by the combination of the solar sail and the low-ballistic-coefficient aerocapture.

In the present study, we consider a Saturn orbiter mission. The major research objectives are as follows:

- 1) To present a mission scenario and the vehicle concept for the nearly-fuel-free planetary exploration by the combination of the solar sail and the low-ballistic-coefficient aerocapture,
- 2) To establish a design methodology of such vehicles including the trajectory analysis, the coupled analysis of the flow field and the membrane structure, and the system analysis,
- 3) To obtain the appropriate vehicle configuration for a small Saturn orbiter with the mass of 300 kg,
- 4) To demonstrate the advantages of the present concept in comparison with other vehicle concepts, that is, an all-propulsive vehicle and an aerocapture vehicle with conventional rigid aeroshell.

2. MISSION CONCEPT

Saturn is the sixth planet of the solar system and famous for its ring system. The composition of Saturn’s atmosphere (about 96% hydrogen, 3% helium and minor species) is believed to be similar to that of the primordial solar nebula, from which our solar system has been formed. Hence, the in-situ exploration from Saturn’s orbit is expected to give us keys to understand the origin of the solar system and also the origin of life, considering the interesting analogy between Saturn’s ring system and the solar system before formation of the planets, and the analogy between Titan (Saturn’s largest moon) and the earth. However, it is quite difficult to realize the in-situ exploration of the outer planets mainly because of the mission cost. Hence, there is a great need for smaller and less-expensive technologies for the planetary exploration probes.

In the present study, we choose Saturn as the target planet for “nearly-fuel-free” exploration mission to demonstrate the advantage of the combination of the solar sail and the low-ballistic-coefficient aerocapture. The mission concept is shown in Figure 1. The sail is stowed at the launch phase and is deployed by the centrifugal force of the spin motion of the vehicle before the interplanetary cruise. During the cruise phase, the flat disk-like shape to make specular reflection of the solar radiation is sustained by the centrifugal force due to the spin. Before the atmospheric entry of the aerocapture, the hoop support is set to be prepared for the aerodynamic force acting on the sail. In the present study, an inflatable torus is considered as the hoop support. The spacecraft mass is assumed to be 300 kg at Saturn just before the orbit insertion. A sequence of events for the aerocapture is as follows:

- (1) The hoop support is set before the atmospheric entry,
- (2) The spacecraft approaches to the planet on a hyperbolic trajectory and enters the atmosphere at an appropriate flight path angle,
- (3) The drag force acting on the sail continues to decelerate the spacecraft during the atmospheric flight,
- (4) The sail is jettisoned when sufficient deceleration has been obtained. After that, the drag force becomes discontinuously and significantly reduced.
- (5) After the atmospheric pass, the periapsis raise maneuver is conducted at the apoapsis to put the spacecraft out of the atmosphere and to avoid further deceleration due to the aerodynamic drag.

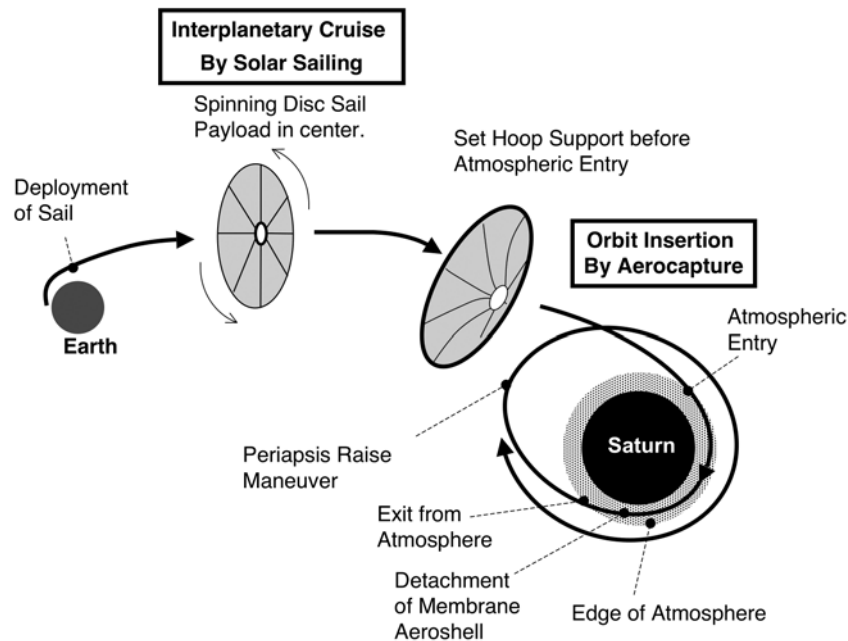


Figure 1. Mission concept of nearly-fuel-free planetary exploration using solar sail and low-ballistic-coefficient aerocapture

It should be noted that the detachment of the sail enables the vehicle to make the drag modulation in a simple and reliable way. By setting an appropriate time for detachment, the spacecraft can be inserted into the desired orbit in a single atmospheric pass even in the presence of the uncertainty in the atmospheric properties.

Figure 2 shows the configuration of the spacecraft during the atmospheric flight of the aerocapture. For the solar sailing, various sail architectures are considered, for example, square sail with the diagonal booms, spinning disk sail without the supporting booms, hoop-supported sail and so on [4]. Considering that the sail must be kept flat and normal to the freestream to produce the aerodynamic force efficiently, some support structure is necessary. The outer edge of the sail should be fastened to it to avoid fluttering. Consequently, we choose the hoop-supported type with the inflatable torus, as shown in Figure 2, from a viewpoint of the structural strength and the mass. After sizing process explained later, the diameter of the disk-like sail before deformation and the tubular diameter of the torus are determined as 100 m and 2.5 m, respectively. The polyimide film is chosen for the material of both the sail and the torus support because of its small density and high heat-resistance. For example, Kapton® is commercially available and its maximum service temperature is higher than 670 K. In the present study, we assume the film material with the tensile strength 300 MPa, the maximum service temperature 770 K, Young's modulus 3.5 GPa, the Poisson's ratio 0.3, the bulk density 1420 kg/m³ and the thickness 5 or 7.5 μm . The main body with the diameter 2 m is located at the center of the sail to carry the spacecraft system and payload. During the atmospheric flight, the sail is deformed into the conical shape with the main body at the apex as shown in Figure 2. As a result, the static stability is expected with respect to the pitch and yaw motions during the atmospheric flight.

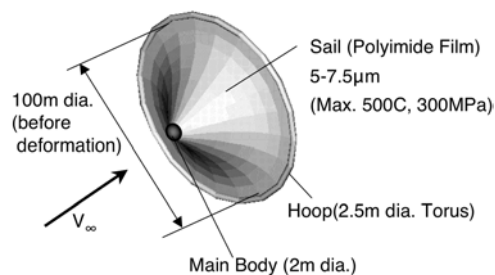


Figure 2. Vehicle configuration during atmospheric flight of aerocapture

3. DESIGN METHODOLOGY

The summary of the design methodology for the present sail vehicle is illustrated in Figure 3. It is mainly separated into three parts: 1) the trajectory analysis and vehicle sizing, 2) flow and structural analysis, and 3) the system design and evaluation. The detail of the method is described in Refs. [8, 9].

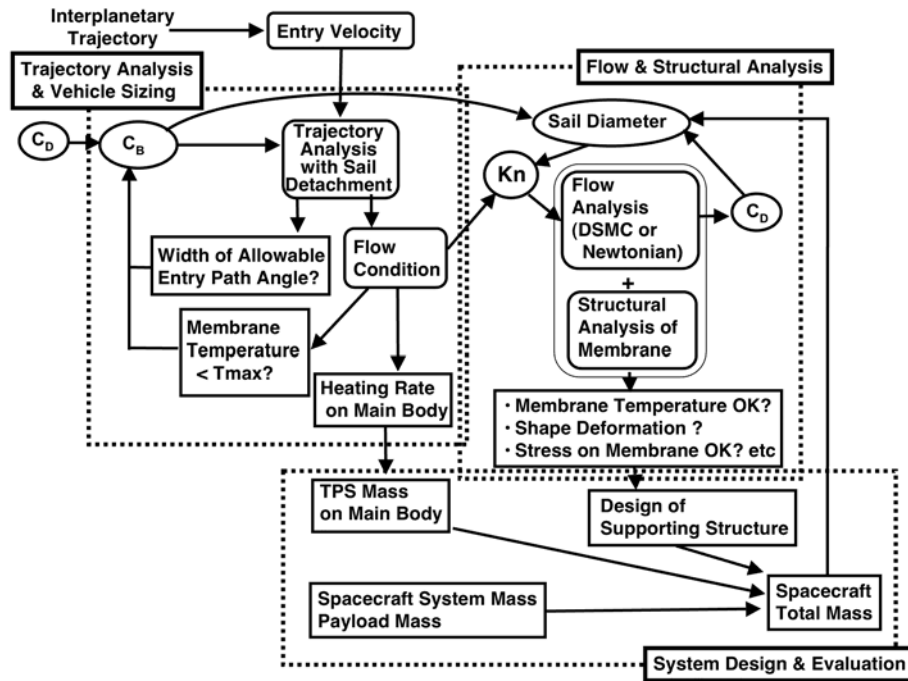


Figure 3. Design methodology of nearly-fuel-free planetary exploration vehicle using solar sail and low-ballistic-coefficient aerocapture

3.1 Trajectory Analysis and Vehicle Sizing

The key parameter in the sizing process is the ballistic coefficient. An aerocapture vehicle with smaller ballistic coefficient can obtain necessary deceleration by flying at higher altitudes and the aerothermodynamic environment around the spacecraft will become more relaxed from a viewpoint of the aerodynamic heating and the stress on the sail. The trajectory analysis is conducted assuming the motion of the point mass on the two-dimensional plane. We determine the appropriate ballistic coefficient considering the following checkpoints:

- (a) The corridor width of the allowable entry path angle,
- (b) The maximum surface temperature of the sail,
- (c) The maximum stress on the sail.

In the present study, the shape of the sail is axially symmetric with respect to the freestream direction as shown in Figure 2 and the lift force is not considered. Once the ballistic coefficient, the entry condition and the atmospheric model are determined, the flight trajectory is uniquely calculated. The time for the sail detachment is determined to obtain the designated exit condition. The entry velocity is set as 35.5 km/s, which corresponds to that of the direct entry from the interplanetary trajectory of the Hohmann transfer [10]. To consider the effect of the uncertainty in the atmospheric model, the maximum and minimum density models are defined from Ref. 11 as shown in Figure 4, assuming that the ratio of the maximum possible density to the minimum possible density is 1000 at 1000 km altitude. The corridor for the entry path angle is defined as the range of the entry path angles, at which the spacecraft can go out of the atmosphere with the required exit velocity both in the case of the maximum possible atmospheric density and in the case of the minimum possible atmospheric density. When the corridor width is too narrow, successful aerocapture will become impossible within the control accuracy at the present state of the art.

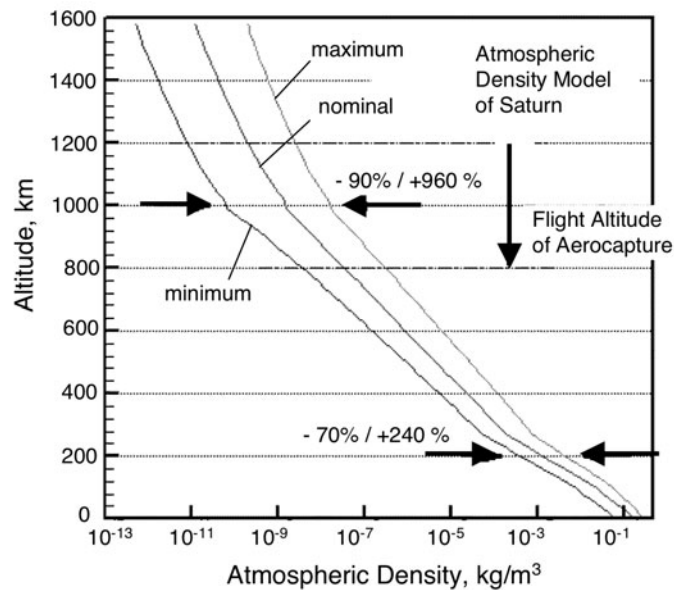


Figure 4. Atmospheric density model of Saturn

In the vehicle sizing part, the detailed flow field analysis is not necessary. For simplicity of analysis, we calculate the aerodynamic heating rate by the free molecular flow model [12]. The sail is assumed to be flat and normal to the freestream direction. The equilibrium temperature on the sail and the main body is calculated by considering the radiative cooling from both sides of the sail and from an open side of the body, respectively. The thermal accommodation coefficient and the emissivity are 1.0 and 0.9, respectively. The assumption of the free molecular flow is not so far from the reality, because the low-ballistic-coefficient aerocapture vehicle flies at relatively high altitudes and the Knudsen number will be higher than 0.1. When the spacecraft main body with the sail detached or the aerocapture vehicle with the conventional rigid aeroshell dives into the atmosphere at the altitude lower than 800 km, Tauber's empirical relation [13] is used to estimate the wall heating rate in place of the free molecular model. The maximum sail temperature along the atmospheric flight trajectory must be lower than the maximum service temperature of the membrane material. The mass of the thermal protection system on the main body is estimated from the aerodynamic heating rate in the system design part.

To reduce the aerodynamic heating to the allowable level, the spacecraft must fly at high altitudes with the low ballistic coefficient. As a result, the pressure acting on the sail is also low and the tensile stress on the membrane is not critical, as shown in the coupled analysis of the flow field and the membrane structure. Consequently, among the above three checkpoints, the most severe one is (a) corridor width of the allowable entry path angle in determining the appropriate ballistic coefficient. Once the ballistic coefficient is determined, the diameter of the sail is calculated assuming the spacecraft mass (300 kg) and the drag coefficient (2.0).

3.2 Coupled Analysis of Flow Field and Membrane Structure

To ensure 1) the sail vehicle can survive under the aerodynamic heating and the stress due to the aerodynamic force during the atmospheric flight of the aerocapture, 2) the necessary drag force is produced by the sail and 3) the hoop of the inflatable torus can successfully support the sail configuration, the coupled analysis of the flow field and the membrane structure is conducted. For the flow field analysis, the Direct Simulation Monte Carlo (DSMC) method [14] is used, because from the results of the trajectory analysis, the Knudsen number based on the sail diameter is higher than 0.03 and the flow around the sail is classified into the rarefied flow regime. For the membrane structure analysis, the particle-based model [2] is used because of its robustness and small computation time. When the aerodynamic pressure acts on the membrane, the shape of the sail changes and the flow around the sail also changes. Consequently, the flow field analysis and the membrane structure analysis must be carried out in a coupled manner as shown in Figure 5.

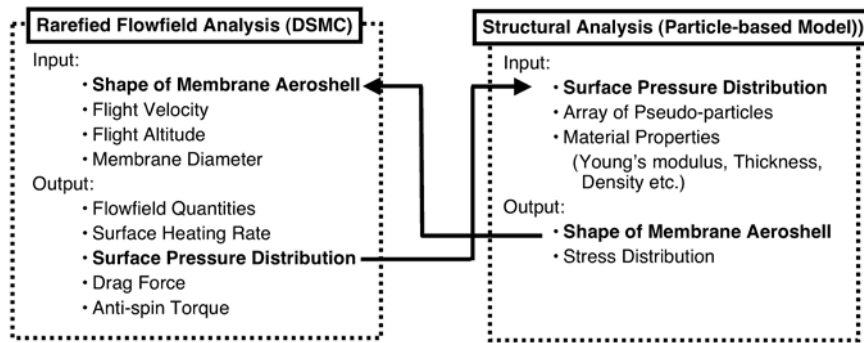


Figure 5. Coupled analysis of flow field around sail and membrane structure

The shape of the sail is determined by the balance among the aerodynamic force, the centrifugal force caused by the spin motion and the elastic force on the membrane. The dynamics of the membrane is numerically simulated by the particle-based model [2], assuming the axisymmetric shape of the sail. In this model, the membrane is described as a network of the pseudo-particles, each of which represents a small element of the membrane, as shown in Figure 6. In this method, the equation of motion is solved for each particle. The equation of motion consists of the inertial force, the aerodynamic force acting normal to the surface, the longitudinal elastic tensile force, the circumferential elastic tensile force, and the centrifugal force acting normal to the spin axis. The resultant of the circumferential stress acts normal to the axis of symmetry. The elastic forces are determined from the positions of the neighboring particles. In the present study, the membrane and the torus are described by using 20 and 20-30 particles in the radial direction, respectively.

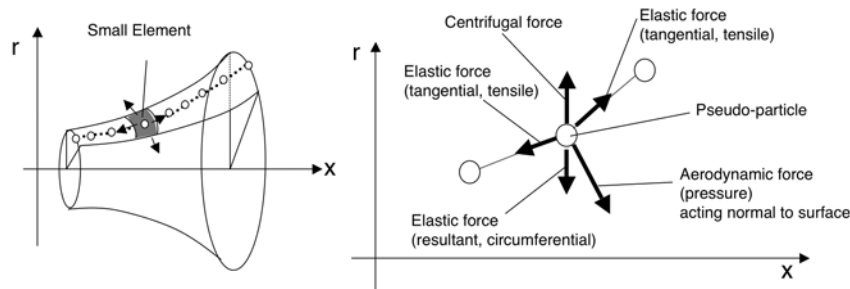


Figure 6. Axisymmetric particle-based membrane model

Though the axisymmetric shape is assumed in the structure analysis, the three-dimensional analysis with the DSMC method is performed for the flow field to avoid the numerical difficulty due to the topological singularity of the symmetry axis. To describe the Saturn's atmosphere of hydrogen molecule, the hard sphere model with the diameter 2.8×10^{-10} m is assumed. At the sail surface, the diffusive wall model at temperature 500 K is used. For the collision calculation, the maximum collision number method [15] is used because of its relatively small computation time. Figure 7 shows the computational cell system. The sail is described by using 220 panels (11 in radial direction and 20 in circumferential direction). The shape of the hoop support is simplified into a flat circular brim around the sail. The sub-grid system ($10 \times 16 \times 16$ cells) is generated around the sail. The sub-grid system is put in the main grid system ($40 \times 40 \times 40$ cells), whose size is 6 times larger than the sail diameter. The particles enter the computational domain according to the freestream condition determined by the trajectory analysis. The number of particles in the computational domain is about 500,000. The aerodynamic heating rate and pressure are calculated from the energy loss and momentum loss at the collision between the particle and the surface, respectively.

3.3 System Design and Evaluation

After the coupled analysis of the flow field and membrane structure, the tubular diameter of the torus and the inflating pressure are determined to avoid intolerably large change in the sail shape, and for the

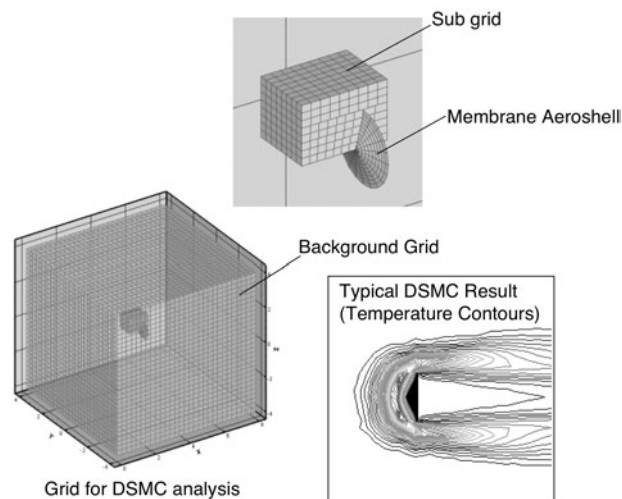


Figure 7. Grid system for DSMC calculation

sail to produce appropriate drag force during the aerocapture. In the present study, the total mass of the spacecraft just before the insertion to Saturn's orbit is assumed to be 300 kg. In case of the aerocapture, the mass of the membrane and the torus from the total mass of 300 kg leaves the mass allotted for the spacecraft system, structure and payload, when the fuel for the periapsis raise maneuver is negligible.

The apoapsis radius of the target orbit is assumed to be 180,000 km, which corresponds to the inner radius of E-ring of the Saturn's ring system. To achieve this orbit insertion from the interplanetary trajectory, the spacecraft velocity must be reduced by 5.2 km/s. To compare with the sail aerocapture vehicle and to demonstrate its advantage, two types of spacecraft are considered: an all-propulsive vehicle and a vehicle with propulsive interplanetary transfer and the orbit insertion by the aerocapture. In the former case, the spacecraft mass at the departure from the low earth orbit is calculated from the summation of the delta-V's for the Hohmann transfer and the orbit insertion at Saturn. The specific impulse of the rocket is assumed to be 312 s. In the latter case, the fuel mass for the orbit insertion at Saturn is not necessary. However, the additional mass for the thermal protection during the atmospheric flight of the aerocapture must be taken into account. When the ablator is used for the thermal protection, the ratio of the TPS mass to the total mass is empirically given by [16]:

$$\frac{TPS\ mass}{Total\ mass} = 0.091 (Heat\ Load[J/cm^2])^{0.51575}, \quad (2)$$

where the heat load is calculated by integrating the stagnation-point aerodynamic heating rate with respect to the time along the atmospheric flight trajectory. In case of the sail aerocapture, the ballistic coefficient is very low and the aerodynamic heating is not so severe even at the stagnation point of the main body. Hence the TPS mass is negligible.

The propellant mass for the combination of the solar sail and the aerocapture is negligible during both the interplanetary cruise and the orbit insertion. The spacecraft mass at Saturn arrival is basically the same as that at the departure from the low earth orbit, except small amount of the propellant for the attitude control, some minor trajectory maneuvering and so on. This is a great advantage of the solar sail over the conventional propulsive orbital transfer vehicle. However, the flight performance of the solar sail strongly depends on the ratio of the sail area to the spacecraft mass. A heavy sail cannot gain necessary acceleration from the solar radiation. To confirm that the designed sail aerocapture vehicle can reach Saturn from the earth by the solar sailing, the optimization of the solar sail trajectory is carried by the method in Ref. [7], in which the two-body problem of the spacecraft and the sun on the two-dimensional plane is considered. The sail is assumed to be flat and the efficiency of the solar radiation reflection is set as 0.8. The optimum control for the angle between the sail and the solar direction is numerically obtained by the adjoint method to minimize the flight time to Saturn. To generate higher thrust, the spacecraft must get closer to the sun to receive stronger solar radiation. However, the close approach to the sun results in the temperature rise of the sail beyond the maximum service temperature of the membrane material. For the maximum surface temperature not to exceed 770

K, the minimum distance from the sun's center is limited to 37 times larger than the radius of the photosphere.

4. RESULTS AND DISCUSSION

4.1 Determination of Ballistic Coefficient for Aerocapture

Figure 8 shows the effect of the ballistic coefficient on the atmospheric flight trajectory. The entry and the exit velocities are 35.5 km/s and 30.3 km/s at altitude 1600 km, respectively. Three cases of $C_B=0.01 \text{ kg/m}^2$, 0.1 kg/m^2 and 63.7 kg/m^2 are considered. The last one represents the aerocapture vehicle with the rigid aeroshell. In the former two cases, the trajectory at the shallowest entry path angle and that at an entry angle steeper by 0.5 degree are shown. The solid circles represent the time for the sail detachment. It is clear that the sail-type low-ballistic-coefficient aerocapture vehicle can achieve the designated exit velocity for wider range of the entry path angle by adjusting the time for the sail detachment. After the sail detachment, the ballistic coefficient abruptly rises up to the level of the rigid aeroshell vehicle. Hence, steep dive into the atmosphere occurs after the sail detachment. Apparently the flight altitude for the aerocapture increases with the decrease in the ballistic coefficient. When the ballistic coefficient is sufficiently low, the aerodynamic heating is reduced for the sail material to survive. Though the spacecraft main body dives into lower altitudes after the sail detachment, the bottom of the trajectory is still higher than the flight altitude of the rigid aeroshell vehicle. This is a great advantage of the sail aerocapture vehicle from a viewpoint of reduction in the TPS mass.

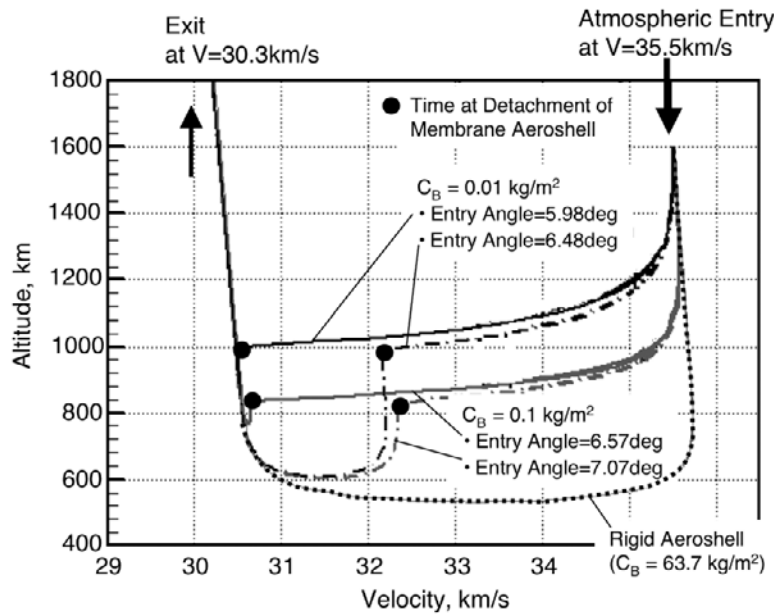


Figure 8. Effect of ballistic coefficient on atmospheric flight trajectory of aerocapture

The corridor width of the entry path angle tends to increase with the decrease in the ballistic coefficient. In addition, as explained in Figure 8, the sail aerocapture vehicle has the capability of the drag modulation by the sail detachment. Figure 9 shows the effect of the entry velocity and the ballistic coefficient on the corridor width of the entry path angle. The delta-V by the aerocapture is set as 5.2 km/s. The corridor width hardly depends on the entry velocity. On the other hand, the corridor width apparently increases with the decrease in the ballistic coefficient. Considering that the control accuracy attainable at the present state of the art is 0.5 degree at best, the ballistic coefficient at the aerocapture must be smaller than 0.1 kg/m^2 . In case of the rigid aeroshell vehicle, the successful aerocapture is almost impossible from a viewpoint of the control accuracy. Consequently, we determine the sail diameter and the tubular diameter of the torus as 100 m and 2.5 m, respectively. In this case, the ballistic coefficient is 0.019 kg/m^2 and the corridor width is 0.92 degree. The compatibility on the surface temperature, the stress on the membrane and the aerodynamic performance is investigated in the next section.

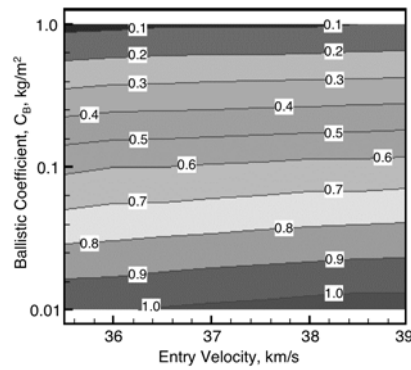


Figure 9. Effect of ballistic coefficient and entry velocity on corridor width of entry path angle

4.2 Sail Aerocapture Vehicle in Atmospheric Flight

As explained in the mission concept, the sail aerocapture vehicle cannot sustain its disk-like shape without the hoop support and/or the spin motion around the axis of symmetry. During the atmospheric flight, the sail vehicle changes its shape from disk type to conical type as illustrated in the upper half of Figure 10. The effect of the inflation pressure of the torus and the spin rate on the displacement of the cone apex, at which the spacecraft main body is located, is shown in Figure 10. The ballistic coefficient, flight velocity and altitude are 0.019 kg/m², 35 km/s and 1100 km, respectively. The thickness of the membrane is assumed to be 5 μm. The displacement diverges and the sail becomes crumpled without the spin and the torus support. In the case without the hoop support, which corresponds to the point at 0 Pa inner pressure in the figure, the displacement is reduced to 20 % of the sail diameter by spinning the vehicle at 15 rpm. On the other hand, without the spin motion, the displacement can be reduced by increasing the pressure in the torus, in other words, by making the hoop support more rigid. When the inner pressure of the torus is higher than 600 Pa and the hoop becomes sufficiently rigid, the displacement becomes almost constant and the effect of the spin disappears. To sustain the shape of the sail, the spin motion seems more favorable than the torus because the latter requires additional mass. However, the friction drag is significant in the rarefied flow regime and the spin motion is rapidly damped in the atmospheric flight. Consequently, the shape of the sail should be sustained mainly by the hoop support with the assist of the spin motion.

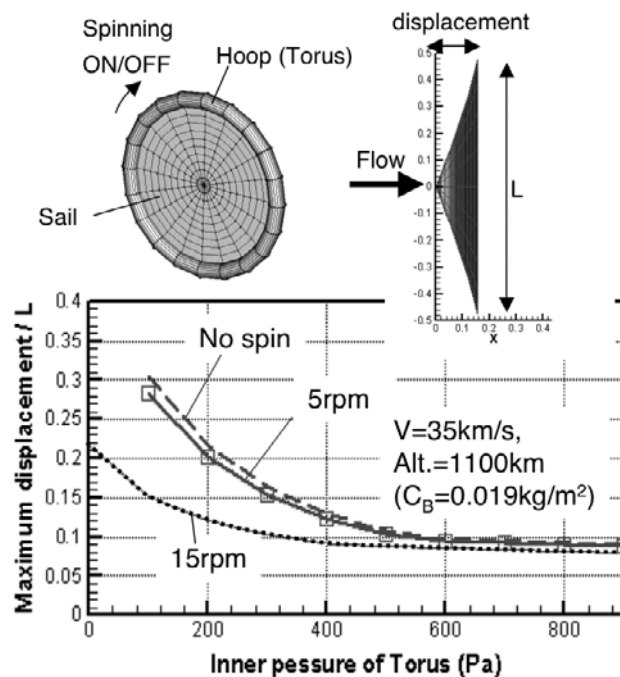


Figure 10. Effect of pressure in torus and spin rate on deformation of sail

When the displacement is large, the shape of the sail changes into a slender cone and the drag force becomes smaller than required for the successful aerocapture. Figure 11 shows the variations of the displacement and the drag coefficient with the altitude along the flight trajectory for the cases of 15 rpm spin only, the torus of inner pressure 200 Pa with 5 rpm spin and 300 Pa torus with 5 rpm spin. The reference area for the drag coefficient is defined as the initial disk area of the sail before deformation. In case of 15 rpm spin only, the drag coefficient continues to decrease as the spacecraft descends in the atmosphere. For the drag coefficient to be always higher than 1.8, the torus must be attached to the rim of the sail.

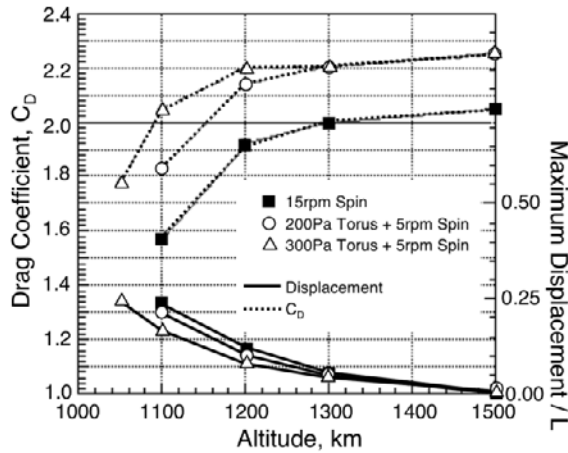


Figure 11. Variation of sail apex displacement and drag coefficient with altitude along flight trajectory

Higher pressure for the inflation of the torus will be better to sustain the shape of the sail and the drag force. However, the stress on the membrane material increases with the inner pressure of the torus. Figure 12 shows the variation of the maximum tensile stress with the inner pressure of the torus and the spin rate. The flight condition is the same as in Figure 10. On the sail, the maximum stress in the radial direction appears at the center of the sail. It increases with the spin rate when the torus is soft with lower inner pressure. In case of higher pressure, the stress becomes almost constant, because the hoop support becomes almost rigid and the stress depends on the aerodynamic pressure. On the torus, the radial stress is much higher than the circumferential stress and they hardly depend on the spin rate. When the inner pressure is lower than 200 Pa, the circumferential stress vanishes and the buckling occurs on the surface of the torus. On the other hand, at the inner pressure higher than 1000 Pa, the radial stress exceeds the tensile strength of the membrane material (300 MPa). Considering the safety margin, the maximum inflation pressure of the torus is 800 Pa.

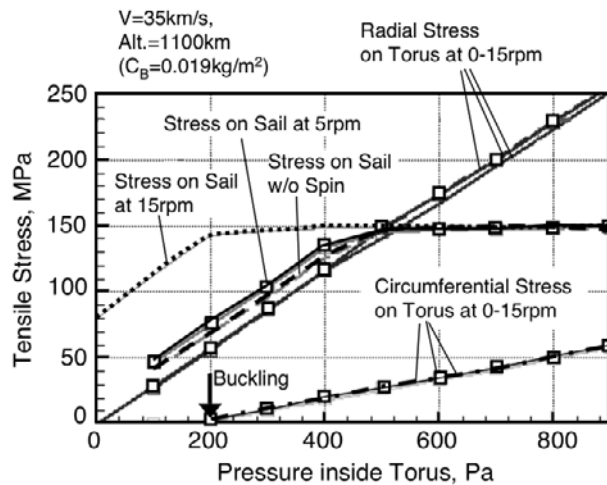


Figure 12. Variation of maximum tensile stress with pressure in torus and spin rate

Figure 13 shows the distribution of the aerodynamic heating rate at various flight conditions. The peak heating is observed at the sail center and the outer edge. As explained in Figure 10, the sail deforms into the conical shape due to the aerodynamic pressure. When the altitude is low and the dynamic pressure is high, the deformation is significant and the peak heating at the apex of the conical shape becomes more severe. However, even at 35 km/s velocity and 1100 km altitude, where the most severe aerodynamic heating is expected, the maximum heating rate is only 7.5 kW/m². In this case, the equilibrium temperature with the radiative cooling from both sides of the membrane is 520 K, which is sufficiently lower than the maximum service temperature of the membrane material. It is demonstrated that the sail aerocapture vehicle can survive under the aerodynamic heating environment because of its high flight altitude due to the extremely low ballistic coefficient.

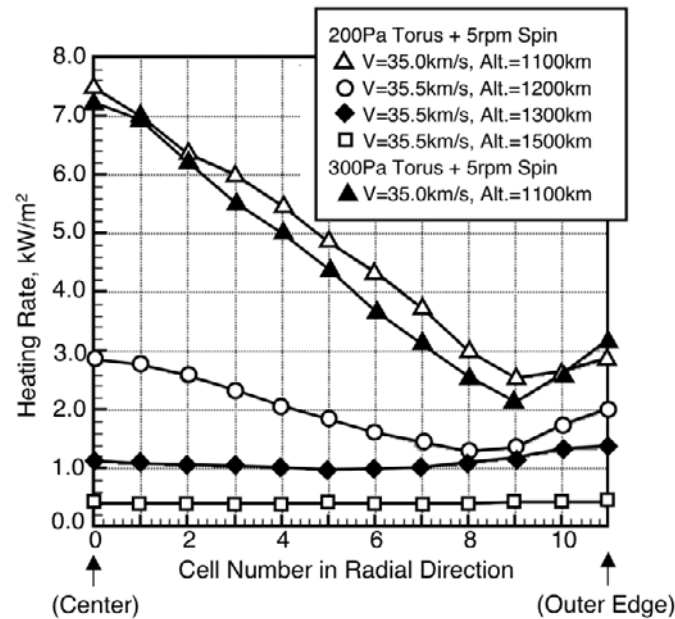


Figure 13. Distribution of aerodynamic heating rate at various flight conditions

4.3 System Design and Evaluation of Sail Aerocapture Vehicle

Before comparing the present sail aerocapture vehicle with the other types of the spacecrafts, it is necessary to assess the performance of the interplanetary flight. The flight performance of the solar sail depends on the mass-to-area ratio. The mass-to-area ratio of the present sail aerocapture vehicle is 38 g/m² and is much higher than that of other solar sail concepts considered so far (10 g/m² or lower). In fact, the trajectory analysis of the solar sailing indicates that the present vehicle cannot reach Saturn without further reduction in the mass-to-area ratio. To do this, we consider that the sail extension made from the advanced thin film material with the density 5 g/m² is attached outside the hoop support as illustrated in Figure 14. When the diameter of the sail extension is 258 m, the mass-to-area ratio becomes 10 g/m². The interplanetary trajectory for the 10 g/m² sail is shown in Figure 14. The trajectory is apparently divided into two parts: the spiral-down to the sun and the spiral-up to Saturn. In this case, it takes 17.1 years from the earth to Saturn. Considering that the flight time is about 6 years in case of the conventional Hohmann transfer, this number seems disappointing. For further reduction in the mass-to-area ratio, the advanced thin film with much lower density per unit area must be developed and used for fabrication of the sail aerocapture vehicle.

Figure 15 shows the comparison of the mass breakdown at the departure from the low earth orbit among the all-propulsive vehicle, the conventional aerocapture vehicle with the propulsive interplanetary orbital transfer and the present sail aerocapture vehicle. The thickness of the membrane is assumed to be 7.5 μm. For all the types of the spacecrafts, the mass at Saturn arrival before the orbit insertion is assumed to be 300 kg. The total mass for the all-propulsive one is about 1250 kg and almost the same as for the conventional aerocapture vehicle, because the reduction in the propellant mass is cancelled by the additional mass for the thermal protection system for the aerodynamic heating during the atmospheric

pass. On the other hand, the total mass for the sail aerocapture vehicle is about 520 kg including the mass for the sail extension shown in Figure 14. It is smaller than 50% of the total mass for the former two types of the vehicle. This fact clearly indicates the advantage of the present “nearly-fuel-free” vehicle concept for planetary exploration from a viewpoint of the spacecraft mass. It enables us to launch the probes to the outer planets with small or medium class launch vehicles with relatively low cost.

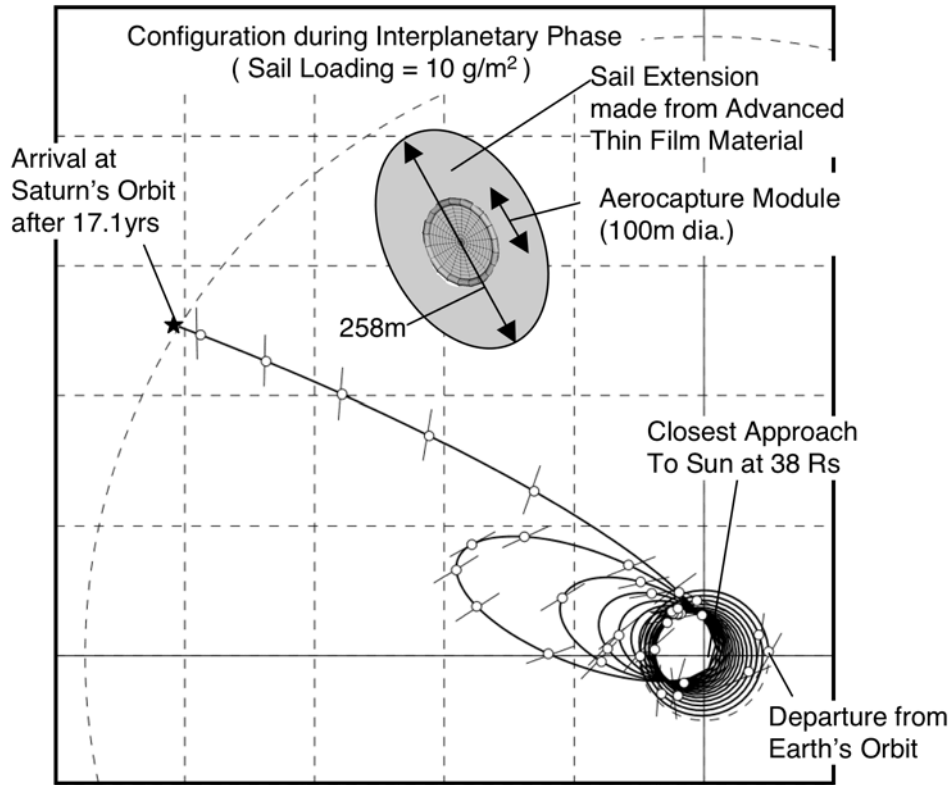


Figure 14. Interplanetary trajectory of solar sailing from earth to Saturn

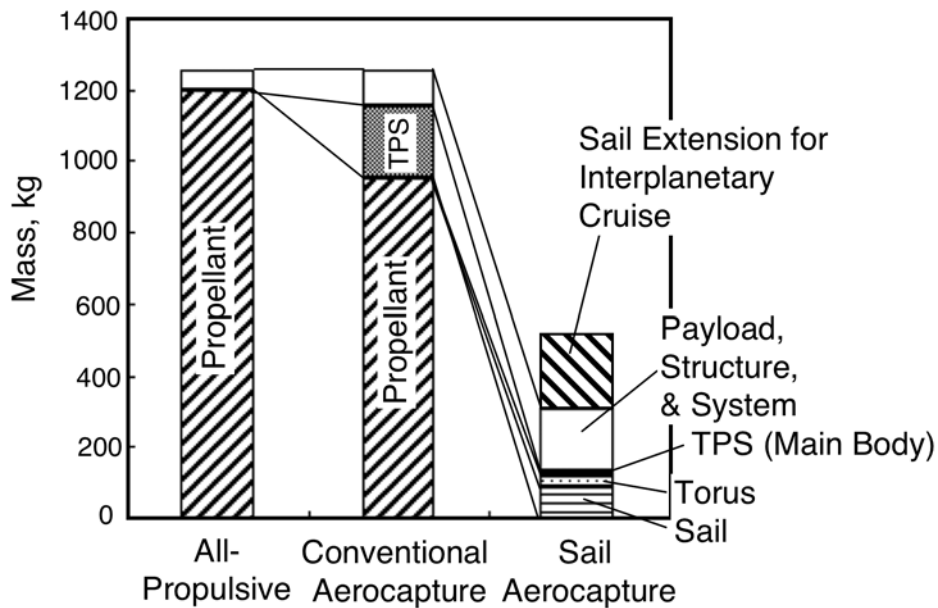


Figure 15. Comparison of mass breakdown among sail aerocapture, conventional aerocapture and all-propulsive vehicles

5. CONCLUSION

In the present study, we propose a novel concept of the nearly-fuel-free planetary exploration by the sail aerocapture vehicle, which uses the sail not only for the solar sailing but also for an aerodynamic decelerator at the orbit insertion. The design methodology is constructed, consisting of 1) the trajectory analysis and vehicle sizing, 2) flow and structural analysis, and 3) the system design and evaluation. Considering a mission to Saturn, the trajectory analysis shows that the corridor of the entry path angle for successful aerocapture is significantly widened and that the aerodynamic heating is much reduced, thanks to the ultra-low ballistic coefficient of the sail-type vehicle. The appropriate ballistic coefficient is mainly determined from the corridor width and the control accuracy. The coupled analyses of the rarefied flow field and the deformation of the sail demonstrate that the solar sail vehicle can survive in the presence of the aerodynamic heating and the stress due to the aerodynamic force. For the vehicle to generate sufficient drag force for successful aerocapture, too large deformation of the sail due to the aerodynamic pressure should be avoided. The hoop support of the inflatable torus with the assist of the spin motion is proposed to sustain the disk-like shape of the sail. By using the sail aerocapture vehicle, the total spacecraft mass at the departure from the low earth orbit can be reduced by more than 50 % in comparison with the all-propulsive vehicle and the aerocapture vehicle with conventional rigid aeroshell. This is a great advantage of the present “nearly-fuel-free” vehicle concept. The problem is intolerably long time for the interplanetary flight by the solar sail, because the present vehicle must survive during the atmospheric flight of the aerocapture and its mass-to-area ratio becomes much larger than the usual solar sail vehicles. To overcome it, the advanced thin film with much lower density per unit area must be developed and used for fabrication of the sail aerocapture vehicle.

REFERENCES:

1. Walberg, G. D. A., Survey of Aero Assisted Orbit Transfer, *Journal of Spacecraft and Rockets*, 1985, 22(1), 3-18.
2. Yamada, K., Suzuki, K. and Hongo, M., Aerodynamic Characteristics of Three-Dimensional Membrane Aeroshells in Supersonic Flow, AIAA Paper 2003-3924, 2003.
3. Suzuki, K., Aerothermodynamic Studies on Low-Ballistic Coefficient Jovian Entry Probe with Membrane Aeroshell, *25th International Symposium on Space Technology and Science (ISTS)*, Kanazawa, ISTS 2006-e-23, 2006.
4. Matloff, G. L., *Deep Space Probes*, Praxis Publishing Ltd., Chichester, UK, 2005.
5. Montgomery IV, E. E. and Johnson, L., The Development of Solar Sail Propulsion for NASA Science Missions to the Inner Solar System, AIAA Paper 2004-1506, 2004.
6. Falkner, P., Berg, M. L., Renton, D., Atzei, A., Lyngvi, A. and Peacock, A., Update on ESA's Technology Reference Studies, *56th International Astronautical Congress*, Fukuoka, IAC-05-A3.4.01, 2005.
7. Colasurdo, G. and Casalino, L., Optimum Control Law for Interplanetary Trajectories with Nonideal Solar Sail, *Journal of Spacecraft and Rockets*, 2003, 40(2), 260-265.
8. Nakamura, K. and Suzuki, K., Aerothermodynamic Analysis on Low-Ballistic-Coefficient Aerocapture Vehicle with Membrane Decelerator, *56th Int. Astronautical Congress*, Fukuoka, IAC-05-E2.2.03, 2005.
9. Nakamura, K., *Feasibility Study on Low-Ballistic-Coefficient Spacecraft for Saturn Exploration*, Master Thesis, The University of Tokyo, 2006 (in Japanese).
10. Hale, F. J., *Introduction to Space Flight*, Prentice-Hall Inc., New Jersey, 1994.
11. Gehrels, T., Matthews, M. S., *Saturn*, The University of Arizona Press, Tucson, Arizona, 1988.
12. Rohsenow, W. M., Hartnett, J. P. and Young, I. C. (ed.), *Handbook of Heat Transfer*, 3rd ed., McGraw-Hill, New York, 1998.
13. Tauber, M. E., Bowles, J. V. and Yang, L., Use of Atmospheric Braking During Mars Missions, *Journal of Spacecraft and Rockets*, 1990, 27(5), 514-521.
14. Bird, G. A., *Molecular Gas Dynamics and The Direct Simulation of Gas Flows*, Oxford University Press, New York, 1994.

- 80 Feasibility study on nearly-fuel-free planetary exploration with low-ballistic-coefficient aerocapture of sail-type vehicle
15. Nanbu, K., Stochastic Solution Method of the Boltzmann Equation II. Simple Gas, Gas Mixture, Diatomic Gas, Reactive Gas, and Plasma, *Institute of Fluid Science Report, Tohoku University, Japan*, 8, 1996, 77-125.
 16. Brown, G. J., Richardson, E., Minimum-Mass Design for Titan Aerocapture, AIAA Paper 2005-1637, 2005.